Data-Driven-Based Vector Space Decomposition Modeling of Multiphase Induction Machines

Mohamed A. Abu-Seif, Mohamed Ahmed, Mohamed Y. Metwly, Graduate Student Member, IEEE, Ayman S. Abdel-Khalik, Senior Member, IEEE, Mostafa S. Hamad, Senior Member, IEEE, and Shehab Ahmed, Senior Member, IEEE, Noha Elmalhy

Abstract—For contemporary variable-speed electric drives, the accuracy of the machine's mathematical model is critical for optimal control performance. Basically, phase variables of multiphase machines are preferably decomposed into multiple orthogonal subspaces based on vector space decomposition (VSD). In the available literature, identifying the correlation between states governed by the dynamic equations and the parameter estimate of different subspaces of multiphase IM remains scarce, especially under unbalanced conditions, where the effect of secondary subspaces sounds influential. Most available literature has relied on simple RL circuit representation to model these secondary subspaces. To this end, this paper presents an effective data-driven-based space harmonic model for n-phase IMs using sparsity-promoting techniques and machine learning with nonlinear dynamical systems to discover the IM governing equations. Moreover, the proposed approach is computationally efficient, and it precisely identifies both the electrical and mechanical dynamics of all subspaces of an IM using a single transient startup run. Additionally, the derived model can be reformulated into the standard canonical form of the induction machine model to easily extract the parameters of all subspaces based on online measurements. Eventually, the proposed modeling approach is experimentally validated using a 1.5 Hp asymmetrical six-phase induction machine.

Index Terms—Multiphase machine, induction motor, machine learning, parameter estimation, six-phase machines.

NOMENCLATURE

x	System state
u	System input
C	Weighted coefficients
Θ	Library of functions
i	Current
v	Voltage
λ	Flux linkage
R	Winding resistance
L	Self or magnetizing inductances
L_l	Leakage inductance
p	Number of pole pairs
n	Number of stator phases
T_e	Developed torque
ω_e	Electrical angular speed
T_d	Developed torque
T_L	Load torque

Subscripts

α, β	Fundamental subspace components
x, y	Secondary subspace components
$0^+, 0^-$	Zero subspace components
s	Stator
r	Rotor
k	Subspace
ph	Phase
seq	Sequence component

Superscripts

s	Stator
r	Rotor
m	Mutual/Magnetizing

Mohamed A. Abu-Seif, Ayman S. Abdel-Khalik and Noha Elmalhy are with the Electrical Engineering Department, Alexandria University, Alexandria 21544, Egypt, (e-mail: mohamedashrf2021@alexu.edu.eg, ayman.abdel-khalik@alexu.edu.eg, noha.elmalhy@alexu.edu.eg).

Mohamed Ahmed is with the Engineering Mathematics and Physics Department, Faculty of Engineering, Alexandria University, Alexandria 21544, Egypt, (e-mail: mohamed.abuyehia@alexu.edu.eg).

Mohamed Y. Metwly is with the Electrical Engineering Department, Alexandria University, Alexandria 21544, Egypt, and is also with Electrical and Computer Engineering Department, University of Kentucky, Lexington 40503, KY, USA, (e-mail: m.metwly@smartci.alexu.edu.eg).

Mostafa S. Hamad is with the Research and Development Center, Arab Academy for Science, Technology and Maritime Transport, Al Alamein 5060305, Egypt (email: mostafa.hamad@staff.aast.edu)

Shehab Ahmed is with the CEMSE Division at King Abdullah University of Science and Technology, Saudi Arabia (email: shehab.ahmed@kaust.edu.sa)

I. INTRODUCTION

In modern variable-speed electric drives, small mismatches between the controller and machine mathematical model may deteriorate the controller performance. Therefore, numerous parameter estimation techniques have been presented in the literature for both three-phase and multiphase induction machines [1-6]. Multiphase machines have shown promise in high-power safety-critical applications since they offer improved fault-tolerance capability, lower per-phase current ratings, and enhanced air gap flux distribution [7, 8]. On the other hand, multiphase machines entail a more complex controller and converter. Amongst multiphase machines, those with multiple three-phase windings are more common than machines with prime phase order since commercial off-the-

shelf three-phase power converters can simply be employed [9, 10]. Thus, industrial sectors mainly utilize six-phase machines with a spatial phase shift of 30^0 between the two three-phase winding groups, commonly denoted as asymmetrical six-phase (A6P) machine, which offers better flux distribution and enhanced fundamental torque producing component [11, 12].

The multiphase IM modeling has extensively been addressed based on either vector space decomposition (VSD) [13] or double d-q modeling approaches [14]. Although both approaches are mathematically equivalent, VSD-based controllers are the most commonly preferred approach from the dynamical response perspective, where a multiphase machine is decomposed into multiple orthogonal subspaces [15,16]. In the most available literature, it is assumed that machine torque production is dominantly developed by the fundamental $\alpha\beta$ subspace. Whereas the secondary and zero-sequence subspaces are mostly considered as non-flux/non-torque producing subspaces [17]. This has been mainly assumed considering that the flux distribution tends to be more sinusoidal as the number of phases increases [15], which may only be valid under healthy conditions.

In literature, the multifrequency current control has been proposed to compensate the induced harmonic current components mapped to various subspaces [18]. Although the distortion in torque profile can be prevented/minimized by harmonic current compensation, novel winding layouts have also been proposed recently to mitigate space harmonics whether the current waveform is sinusoidal or distorted [19].

On the other hand, modeling the effect of the air gap low-order space harmonics on the multiphase induction machine dynamic behavior remains scarce [15, 20]. Initially, the notable effects of low-order harmonics were considered in the mathematical model of symmetrical six-phase (S6P) IM [21]. As a result, the steady-state six-phase currents were better estimated. Moreover, the influence of the induced third harmonic in the air gap flux has been highlighted for five-phase IM with single layer winding for the open-phase case in [22]. Furthermore, the study given in [20] introduced an improved parameter identification method for A6P IM taking into account the effect of the mutual leakage inductance and rotor induced currents in the zero-sequence subspace. Accordingly, the estimation of the input impedance of the zero-sequence subspace was affected by the induced third harmonic flux component. An improved low-order space harmonics modeling has recently been presented to shed light on the parasitic effects of these harmonics on an A6P IM under different neutral configurations [15]. As a result, it was concluded that the simple harmonic-free model can be utilized for the xy subspace since the effect of the fifth- and seventh-order harmonics mapped to this subspace is very negligible. However, the effect

of the third harmonic mapped to the zero-sequence subspace is notable under unbalanced operation; therefore, the harmonic-free model for this subspace yields a notable inaccuracy during transients. Besides, identifying the parameters of non-fundamental subspaces stands as the main mathematical challenge to include the effect of these secondary subspaces [15, 20]. These parameters are either identified analytically in [20] or using finite element analysis (FEM) in [1].

Multi-objective parameter estimation of IMs has been widely used to match the estimated and manufacturer data [23]. Several methods for three-phase IM have been presented in the literature using a sparse grid optimization algorithm [24], particle swarm optimization (PSO) [25], and a backtracking search algorithm [26]. Other algorithms were used in the literature in order to estimate the full parameters of the three-phase induction machine including the mechanical parameters using polynomial regression [27], and convex optimization [6]. Moreover, a new method based on PSO for multiphase IMs parameter identification has been elaborated in [28]. Interestingly, machine learning (ML) algorithms, a part of artificial intelligence (AI), have recently been used in the date-driven modeling of dynamic systems [29]. Various ML algorithms have also been employed for the diagnosis of induction motors [30, 31]. However, to the best of the authors' knowledge, the employment of ML approaches for multiphase IM dynamic modeling has not been conceived thus far.

This paper introduces an ML-based technique to develop an efficient low-order space harmonic dynamic model for n-phase IMs using the so-called sparse identification of non-linear dynamics (SINDy) approach. This approach can efficiently model both the electrical and mechanical dynamics of the n-phase IMs including the secondary subspaces dynamics using a single transient run (start-up or transient change) without the need for any additional sensors than those already available on the drive itself. Also, this technique can effectively identify the effect of the low-order harmonics that are mapped to the non-fundamental subspaces under unbalanced conditions, which represents the main merit over available models. The effect of neglecting the dynamics of the secondary subspaces is illustrated based on a comparative study in the results section. A comparison of the proposed modeling approach with the available presented models in the literature is summarized in Table I. In addition, the obtained model may be reformed into the canonical form of the induction machine in order to extract the machine parameters, necessitating neither a significant amount of time nor laborious tests. Finally, Experiments have been carried out using a 1.5 Hp asymmetrical six-phase IM to validate the proposed modeling approach.

TABLE I
COMPARISON OF MODELING APPROACHES OF MULTIPHASE IMS

ref	No. of phases	R_s estimation	R_r estimation	$\alpha\beta$ subspace	xy subspace	zero subspace	Technique
[20]	6	√	×	√	√	×	Modified Standard test
[2]	5	√	√	√	×	×	Step voltage at standstill
[32]	n	√	√	√	√	×	Sinusoidal excitation methods
[17]	n	√	×	√	√	×	On-line estimation
Proposed	n	√	√	√	√	√	Data-driven

II. SPARSE IDENTIFICATION OF NONLINEAR DYNAMICS (SINDY) APPROACH

Discovering the governing equations of a dynamical system is, in general, a challenging process. The main objective is to discover the governing equations of a multiphase induction machine with multiple subspaces that correlates its input-output relation. Typically, these equations can be used for either model-based simulation or controller design. Although these equations can accurately describe the system, the derivation of these equations is complex and entails an expert in the loop to highlight the relation between each phenomenon and the corresponding measurement. Further, it requires performing certain measurements on the machine to extract its parameters to fully describe the general model.

Unlike system modeling based on dynamical equations, data-based modeling, e.g., neural network architecture, has recently emerged to model complex systems with high accuracy. The data-based modeling might result in more accuracy; however, it is complex, less controllable, and doesn't necessarily give any physical meaning to the system itself. For analyzing and controlling the multiphase machines, the generated models need to be in the form of linear or nonlinear differential equations. A new technique offering the merits of both modeling approaches has been developed, namely, sparse identification of nonlinear dynamics (SINDy) [33]. This approach provides a straightforward data-driven framework to model the system from data measurement and results into a model in the form of differential equations.

The only assumption about the model structure is that a few important terms are used to govern the dynamics so that the equations are sparse in the space of possible functions. For example, the current is proportional to the voltage in the electric machine; therefore, the algorithm will result in a model that is a function of these variables.

By using SINDy, it is required to determine a set of differential equations in the form of $dx(t)/dt = f(x(t), u)$, where x represents the system states and u represents the system inputs. In case of induction machines, the machine states are currents, or fluxes, and speed, while the reference inverter voltages are the system inputs. So, it is necessary to collect the time history of the state $x(t)$ and measure the derivative $\dot{x}(t)$ or approximate it numerically from $x(t)$. The data are sampled at various intervals t_1, t_2, …, and t_m and organized into two matrices as in (1) and (2).

$$\mathbf{X} = \begin{bmatrix} x^T(t_1) \\ x^T(t_2) \\ \vdots \\ x^T(t_m) \end{bmatrix} = \begin{bmatrix} x_1(t_1) & x_2(t_1) & \cdots & x_N(t_1) \\ x_1(t_2) & x_2(t_2) & \dots & x_N(t_2) \\ \vdots & \vdots & \ddots & \vdots \\ x_1(t_m) & x_2(t_m) & \dots & x_N(t_m) \end{bmatrix} \quad (1)$$

$$\dot{\mathbf{X}} = \begin{bmatrix} \dot{x}^T(t_1) \\ \dot{x}^T(t_2) \\ \vdots \\ \dot{x}^T(t_m) \end{bmatrix} = \begin{bmatrix} \dot{x}_1(t_1) & \dot{x}_2(t_1) & \cdots & \dot{x}_N(t_1) \\ \dot{x}_1(t_2) & \dot{x}_2(t_2) & \dots & \dot{x}_N(t_2) \\ \vdots & \vdots & \ddots & \vdots \\ \dot{x}_1(t_m) & \dot{x}_2(t_m) & \dots & \dot{x}_N(t_m) \end{bmatrix} \quad (2)$$

where N is the number of states. A matrix $\Theta(\mathbf{X})$ consisting of candidate non-linear functions of the columns of $\mathbf{X}$ and input vectors is then constructed. For example, $\Theta(\mathbf{X})$ may consist of constant, polynomial, and trigonometric terms. This matrix represents the possible correlation between the states and the inputs and is described as follows:

$$\Theta(\mathbf{X}) =$$
$$\begin{bmatrix} \overbrace{\vdots \quad \quad \vdots}^{k \text{ input vectors}} & & & & & & \\ u_1 & \dots & u_k & 1 & \mathbf{X} & \mathbf{X}^{P_2} & \mathbf{X}^{P_3} & \dots & sin(\mathbf{X}) & cos(\mathbf{X}) & \dots \\ \vdots & & \vdots & \vdots & \vdots & \vdots & \vdots & & \vdots & \vdots & \end{bmatrix}$$
$$(3)$$

Higher polynomials are indicated as $\mathbf{X}^{P_2}$, $\mathbf{X}^{P_3}$, etc., where $\mathbf{X}^{P_2}$ represents the quadratic nonlinearities in the state x and is described as follows,

$$\mathbf{X}^{P_2} = \begin{bmatrix} x_1^2(t_1) & x_1(t_1)x_2(t_1) & \dots & x_2^2(t_1) & \dots & x_N^2(t_1) \\ x_1^2(t_2) & x_1(t_2)x_2(t_2) & \dots & x_2^2(t_2) & \dots & x_N^2(t_2) \\ \vdots & \vdots & \ddots & \vdots & \ddots & \vdots \\ x_1^2(t_m) & x_1(t_m)x_2(t_m) & \dots & x_2^2(t_m) & \dots & x_N^2(t_m) \end{bmatrix} \quad (4)$$

The SINDy objective is to find which candidate functions can optimally model the system. Sparse regression therefore aims to identify a set of vectors comprising weighted coefficients $\mathbf{C} = [\, c_1 \; c_2 \; \cdots \; c_N \,]$. These coefficients describe the weight of each nonlinearity in the model and which of those are effective. The sparse regression problem is formulated as follows,

$$\dot{\mathbf{X}} = \Theta(\mathbf{X})\mathbf{C} \quad (5)$$

Each column c_k of $\mathbf{C}$ is a sparse vector of coefficients determining which terms are effective in the right-hand side for one of the dynamic equations $\dot{x}_k(t) = f(\mathbf{x}_k(t), u)$ in (1). Once $\mathbf{C}$ is constructed, an accurate depiction of the system dynamics can be obtained, which describes all possible candidate functions of the system. For example, the machine speed voltage is a nonlinear term that represents the product of linkage flux and angular speed. This can simply be modeled as a second-degree polynomial. The sparse regression problem will then disregard all the other possible terms except the term $\lambda\omega_r$.

The main advantage of SINDy in modeling electrical systems is that it does not require a certain structure of predetermined equations to describe the system model. This fact opens the door for modeling any non-linear behavior of the machine from several perspectives, such as the magnetic behavior, temperature, change of parameters, and so on. These effects can accurately be modeled as long as the correct data that contains enough information and transients is provided.

III. MODELLING PROCEDURES OF IMs USING SINDY

This section introduces the procedures of the proposed modeling approach for multiphase IMs. First, the required mathematical representation of IMs is presented. After that, the main steps of the proposed data-driven modeling are described in detail.

It is well-established in the available literature that the governing dynamic equations can sufficiently be represented using the dominant low-order space harmonics in different subspaces [15]. Harmonics of higher order will consequently be ignored in this paper. The general assumptions that will also be made are as follows:

1) The magnetic circuit is assumed linear, and the effect of hysteresis, as well as eddy current losses, will be

discarded. Saturation yields the same model formulation, however, it affects the model parameters, as well be shown in the results section.

2) The effect of slot harmonics is neglected.
3) All sources of winding asymmetries will be ignored.

Based on these assumptions, the $\alpha\beta$ subspace will be responsible for the fundamental torque producing flux component, the xy subspace will represent the effect of the 5th and 7th space harmonics, and the $0^+, 0^-$ subspace will account for the effect of the air gap third harmonic flux component.

A.   Space Phasor Modeling of IMs

An *n*-phase induction machine is commonly modelled using VSD modelling, where the phase variables vector, $\mathbf{y}_{ph}$ is decomposed into *n* sequence components using the orthogonal transformation given by (6) and detailed in [34].

$$\mathbf{y}_{seq} = \mathbf{T}_n \mathbf{y}_{ph} \tag{6}$$

where $\mathbf{T}_n$ is the VSD transformation matrix.

The machine voltage equations in space phasor form for any subspace *k* are therefore given by (7) and (8), while the stator and rotor flux linkage equations are given by (9) and (10), respectively.

$$\underline{v}_k^s = (R^s \underline{i}_k^s + \frac{d\underline{\lambda}_k^s}{dt}) \tag{7}$$

$$0 = R_k^r \underline{i}_k^r + \frac{d\underline{\lambda}_k^r}{dt} - j\omega_e \underline{\lambda}_k^s \tag{8}$$

$$\underline{\lambda}_k^s = L_k^s \underline{i}_k^s + L_k^m \underline{i}_k^r \tag{9}$$

$$\underline{\lambda}_k^r = L_k^r \underline{i}_k^r + L_k^m \underline{i}_k^s \tag{10}$$

where R^s and R_k^r are the resistances of the stator and rotor, respectively. L_k^s and L_k^r are the self-inductances of the stator and rotor, respectively, and L_k^m is the mutual inductance between stator and rotor.

Since rotor currents are usually unmeasurable, the model is reformulated using stator variables only, namely, stator current and flux components. From (9) and (10), then,

$$\underline{i}_k^r = -\frac{L_k^s}{L_k^m} \underline{i}_k^s + \frac{1}{L_k^m} \underline{\lambda}_k^s \tag{11}$$

$$\underline{\lambda}_k^r = -\frac{\sigma_k L_k^s L_k^r}{L_k^m} \underline{i}_k^s + \frac{L_k^r}{L_k^m} \underline{\lambda}_k^s \tag{12}$$

where the leakage factor $\sigma_k = 1 - (L_k^m)^2 / L_k^r L_k^s$

Substituting from (7), (11), and (12) in (8) gives the following state equation in space phasor form.

$$\frac{d}{dt} \underline{i}_k^s = -\left(\frac{R_s L_k^r + R_k^r L_k^s}{\sigma_k L_k^r L_k^s}\right) \underline{i}_k^s + \frac{1}{\sigma_k L_k^s} \underline{v}_k^s$$

$$+ \frac{R_k^r}{\sigma_k L_k^r L_k^s} \underline{\lambda}_k^s + j\omega_e \underline{i}_k^s - j \frac{1}{\sigma_k L_k^s} \omega_e \underline{\lambda}_k^s \tag{13}$$

The stator flux components can be estimated from the integration of (7). This integration, however, depends on the stator resistance, which can simply be obtained from the dc resistance test.

The remaining state equation is the mechanical equation, which is given by,

$$\frac{d\omega_e}{dt} = -\frac{b}{J} \omega_e + p \frac{T_d - T_L}{J} \tag{14}$$

$$T_d = \sum_k^n \frac{n}{2} kp \, real \left(j\underline{\lambda}_k^s \underline{i}_k^{s*}\right) \tag{15}$$

Under asymmetrical six-phase induction machine, which is used for experimental validation, there are three subspaces, namely $\alpha\beta$ ($k = 1$), $xy(k = 5)$ and $0_+0_-(k = 3)$, where k also refers to the dominant harmonic order of the corresponding subspace.

B.   Data Preprocessing

1)   Data filtration

Data filtering is crucial, since motor drives generally generate significant noise levels that might be coupled to the sensors. This noise affects the estimation accuracy, especially when SINDy algorithm calculates the derivatives of these observations.

Another important issue is the possible DC offsets in the output of the current sensors and the corresponding effect on the flux estimation. Fig. 1 describes the discrete Fourier analysis for the experimental current waveform under no-load operation and supply frequency of 50Hz. It is evident that the current spectrum comprises high order component at switching frequency and a DC bias.

The high frequencies are attenuated using an 8th-order band-stop IIR filter (Butterworth) with a lower cutoff frequency of 500 Hz and a higher cutoff frequency of 25kHz. Fig. 2(a) depicts the magnitude and phase responses of the band-stop filter, whereas Fig. 2(b) shows the current response signal during the starting period of the prototype machine before and after filtration to remove high frequency components. To get rid of any DC offset component, an additional high pass IIR filter of order 8 and a corner frequency of 5 Hz is selected. Fig. 3(a) shows the magnitude and phase responses of the employed high pass filter, whereas Fig. 3(b) depicts the current signal before and after applying the filter.

Applying these two filters distorts the frequency phase shift response, as shown in Figs. 2(a) and 3(a). However, by applying the time reversal property of the discrete Fourier transform, the input data x can be processed in both the forward and backward directions. After filtering the input in the forward direction, the function reverses the sequence and filters it again in the backward direction. This process guarantees zero phase distortion or time delay in the filtered signals. This zero-phase digital filtering is performed using the *filtfilt* Matlab function.
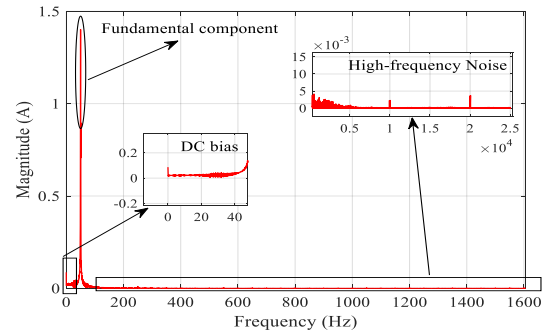
Fig. 1. Discrete Fourier transform of the phase current waveform.
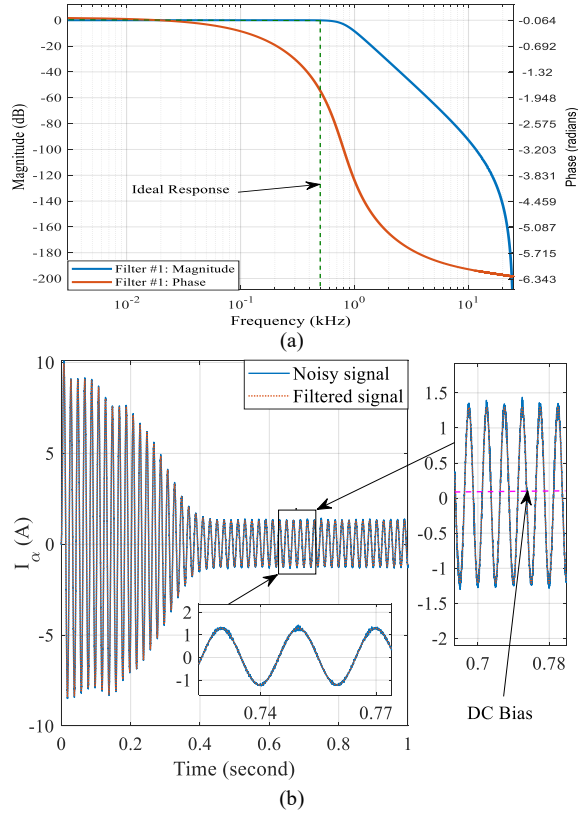
Fig. 2. The characteristics of the Band-stop filter. (a) Magnitude and phase responses of the filter. (b) The current signal before and after filtration of the high frequencies.
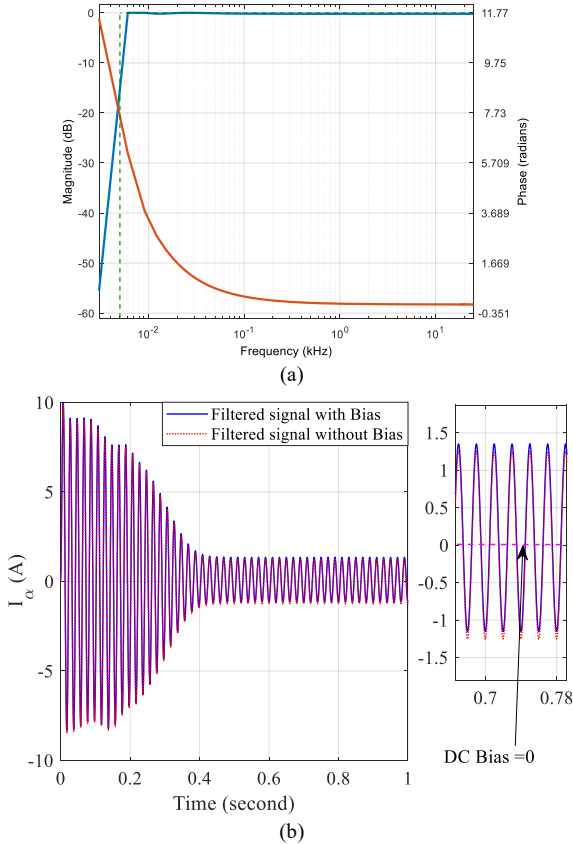
Fig. 3. The characteristics of the High pass filter. (a) Magnitude and phase responses of the filter. (b) The current signal before and after removing the DC bias.

2) Stator Flux Estimation

As a second step, it is necessary to estimate the precise stator flux by integrating (7). Generally, numerical differential equations may be classified into two types depending on the damping term (ζ) in the exact solution ($e^{-\zeta t}$): stiff and non-stiff differential equations, where ζ is a large constant for stiff type and a small constant for the non-stiff type. It is evident from (7) that the flux dynamics is dependent on the current dynamics. Since the current has a relatively small damping factor (seen by the decline of the filtered current waveform after 0.5 seconds in the current response shown in Fig. 3), eq. (7) can be classified as a non-stiff differential equation.

Thereby, (7) can be solved numerically using the fourth order Runge-Kutta method with a proper time step length using (16) and (17). This method gives higher accuracy compared to the conventional integration.

$$d\underline{\lambda}_k^s/dt = f(\underline{v}_k^s, \underline{i}_k^s) = \underline{v}_k^s - R_s \underline{i}_k^s$$

$$\text{with an initial condition } \left(\underline{\lambda}_k^s\right)^0 = f\left(\left(\underline{v}_k^s\right)^0, \left(\underline{v}_k^s\right)^0\right) \quad (16)$$

$$\left(\underline{\lambda}_k^s\right)^i = \left(\underline{\lambda}_k^s\right)^{i-1} + 0.166(k_1 + 2k_2 + 2k_3 + k_4)$$

$$\text{where} \quad k_1 = \Delta t\, f(t^{i-1}, \left(\underline{\lambda}_k^s\right)^{i-1})$$
$$k_2 = \Delta t f(t^{i-1} + 0.5\Delta t, \left(\underline{\lambda}_k^s\right)^{i-1} + 0.5k_1)$$
$$k_3 = \Delta t f(t^{i-1} + 0.5\Delta t, \left(\underline{\lambda}_k^s\right)^{i-1} + 0.5k_2) \quad (17)$$
$$k_4 = \Delta t f(t^{i-1} + \Delta t, \left(\underline{\lambda}_k^s\right)^{i-1} + k_3)$$

3) Data differentiation

Before applying the regression analysis, it is necessary to numerically approximate the derivative of the states $\dot{x}(t)$ from $x(t)$. Forward difference approximation $dx/dt = (x_{n+1} - x_n)/\Delta t$ and backward difference approximation $dx/dt = (x_n - x_{n-1})/\Delta t$ are the most frequent approaches for numerical differentiation; nonetheless, they involve a significant inaccuracy proportional to the step size $O(\Delta t)$. Since the model estimation is highly dependent on the accuracy of the differentiation, it is essential to employ an accurate approach, such as the central difference of second order, whose error is proportional to $O(\Delta t^2)$. The centered difference approximations can be defined as follows:

$$\frac{dx}{dt} = \frac{x_{n+1} - x_{n-1}}{2\Delta t} \quad (18)$$

There are more precise fourth-order $O(\Delta t^4)$ differentiation algorithms, but at the expense of increased computing complexity.

C. Constructing SINDy Model for Multiphase IMs

In order to evaluate the model coefficients, one startup sequence of the machine in the open loop is required. The proposed model is general for any subspace of the multiphase induction machine. To generate this model, a time history of the machine states is collected. These states are the subspace currents after filtration, the filtered mechanical speed, and the estimated stator flux based on the stator currents and input voltage using fourth-order Runge-Kutta method. The

5

appropriate derivatives of the states $\mathbf{X}$ are then computed using the second order central difference approximation. Finally, the library of the non-linear functions $\boldsymbol{\Theta}(X)$ is constructed using only first and second order polynomials. The selection of the non-linear functions is done based on the prior knowledge of the induction machine dynamics and the existence of 2nd order terms (speed voltage terms) in the machine dynamic equations. Moreover, SINDy seeks to minimize the number of the non-zero terms by using an ℓ1-regularized regression [33], resulting into a sparse model constructed from the active terms that contribute to the induction machine dynamics.

As far as the estimation of the fundamental $\alpha\beta$ subspace (dominant torque producing subspace) is concerned, balanced applied voltages can excite this specific subspace, while the effect of other subspaces will be nullified. In order to obtain the dynamical model of all subspaces, unbalanced applied voltages can excite all machine subspaces, which is mandatory for the proposed estimation algorithm.

Fig. 4 depicts the flowchart of the proposed data-driven modeling of multiphase IMs based on SINDy algorithm[1]. While Table II summarizes the main steps of SINDy. In the following section the proposed model is verified and evaluated using a 1.5 Hp prototype asymmetrical six-phase induction machine.

IV Experimental Verification

To verify the effectiveness of the proposed modeling approach, experimental results are conducted using the test setup shown in Fig. 5. A 1.5 Hp induction machine is used with the specification given in Table III and is fed using a six-phase inverter operating at 5kHz switching frequency using sinusoidal pulse width modulation. A 300V programmable dc supply is used as a dc-link. A dSPACE 1202 model is used to derive the six-phase inverter and capture the machine variables (currents and speed). The prototype machine is run under open-loop control. Current measurements are obtained using LEM hall-effect sensors, while an Omron Rotary Shaft Encoder E6B2-CWZ1X is used for the speed measurement. Model validation is carried out under two cases: balanced and unbalanced operation. The former can effectively estimate the $\alpha\beta$ subspace model, while the latter can estimate the models of all subspaces concurrently.

A. Derived Machine Models

In this subsection, the machine model under both balanced and unbalanced cases are derived. The healthy case can sufficiently be used to estimate the fundamental subspace, while the unbalanced case is employed to estimate the secondary subspaces.

Case 1: Balanced six-phase operation

In this case, the machine is driven when balanced six-phase voltages are applied. Under this case, the reference sequence voltages in per unit is $\underline{v}_{\alpha\beta}^s = 0.68\angle 0^0$ at a constant reference frequency of 50Hz, where these values are suggested to reduce the starting motor current to avoid saturating the output of the current measuring board. The reference inverter voltages were utilized as the input voltage to the proposed model, which is

more appropriate for actual drive systems in which just phase currents and speed are measured. Therefore, the suggested model would incorporate the influence of the inverter voltage drop in the dynamic equations. It is worth noting that the machine can be started at any desired frequency, which does not theoretically affect the machine model formulation. The effect of core saturation and frequency is considered in subsequent subsections.

TABLE II
Algorithm 1: Data-driven-based VSD modeling

1:	Run DC test to estimate the stator resistance $R_s = \frac{V_{dc}}{I_{dc}}$.
2:	Startup the machine under open loop control to while machine currents, and speed are measured (i_n, ω_m)
3:	Decompose the machine phase variables into its multiple orthogonal subspaces using the orthogonal transformation given by (6).
4:	Only utilize the transient period since it reflects the system's dynamics. $\underline{v}_k^{t=0:t_1}, \underline{i}_k^{t=0:t_1}, \omega_m^{t=0:t_1}$, where t_1 is the end of the transient period.
5:	Apply the data filtration with the proposed tuning for the quantities in step 4 to successfully remove both the noise and bias and get the filtered quantities.
6:	Apply fourth order Runge-Kutta method to estimate the stator flux $\underline{\lambda}_k^s$ using (7).
7:	Apply the central difference approximations to find the states' derivatives using (18).
8:	Construct the SINDy matrices, which are $\dot{\mathbf{X}}$ and $\boldsymbol{\Theta}(\mathbf{X}, \mathbf{U})$ considering nonlinearities up to polynomial degree two. The states are $\underline{i}_k^s, \omega_m, \underline{\lambda}_k^s$ and the $\underline{v}_k^s$ is an input.
9:	Apply the sequentially threshold least squares (STLS_REGR) to find the optimal $\mathbf{C}$.

l_1 **Function** STLS_REGR $(\dot{\mathbf{X}}, \boldsymbol{\Theta}(\mathbf{X}, \mathbf{U}), \varepsilon)$
l_2 $\quad\mathbf{C}^0 \leftarrow (\boldsymbol{\Theta}^{\mathbf{T}})^\dagger \dot{\mathbf{X}}$ $\quad\triangleright$ initial guess
l_3 $\quad$**while** not converged **do**
l_4 $\quad\quad i \leftarrow i + 1$
l_5 $\quad\quad id_{small} \leftarrow (Abs(\mathbf{C}) < \varepsilon)$ $\quad\triangleright$ find small entries
l_6 $\quad\quad \mathbf{C}^\mathbf{k}(id_{small}) \leftarrow 0$ $\quad\triangleright$ …and Threshold
l_7 $\quad\quad$**for** [f in the range = number of states] **do**
l_8 $\quad\quad\quad id_{large} \leftarrow \sim id_{small}(:, f)$ $\triangleright$ find large entries
l_9 $\quad\quad\quad \mathbf{C}^\mathbf{k}(id_{large}, f) \leftarrow \left(\boldsymbol{\Theta}^\mathbf{T}(:, id_{large})\right)^\dagger \dot{\mathbf{X}}(:, f)$
l_{10} $\quad\quad$**End for**
l_{11} $\quad$**End while**
l_{12} $\quad$**Return** $C_{optimal}$
l_{13} **End function**

10	Validate the results from the model with the experimental results

TABLE III
PROTOTYPE MACHINE SPECIFICATIONS

Parameter	Value	Parameter	Value
RMS phase Voltage (V)	110V	Frequency (Hz)	50
Power (Hp)	1.5	No. of poles	4
RMS phase current (A)	2.8	Speed (RPM)	1400

---

[1] The Matlab m-files implementation of the scheme proposed in Fig. 4 is available as a supplementary material of this paper.
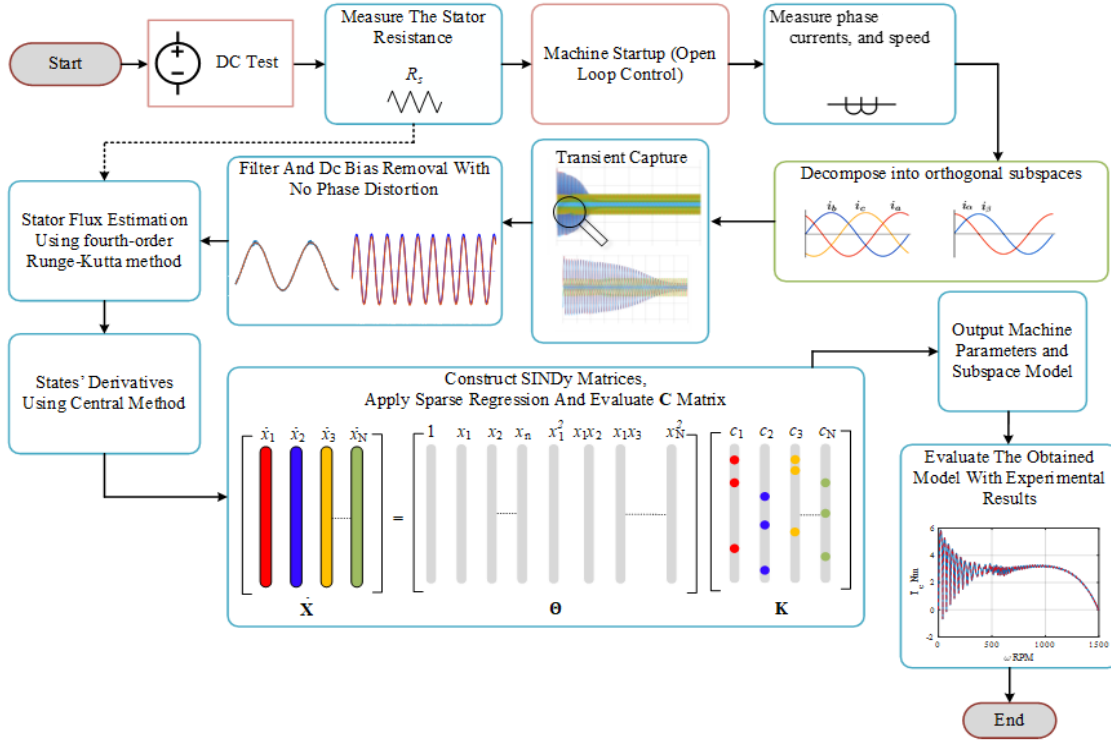
Fig. 4.   Flowchart of the proposed modeling approach.
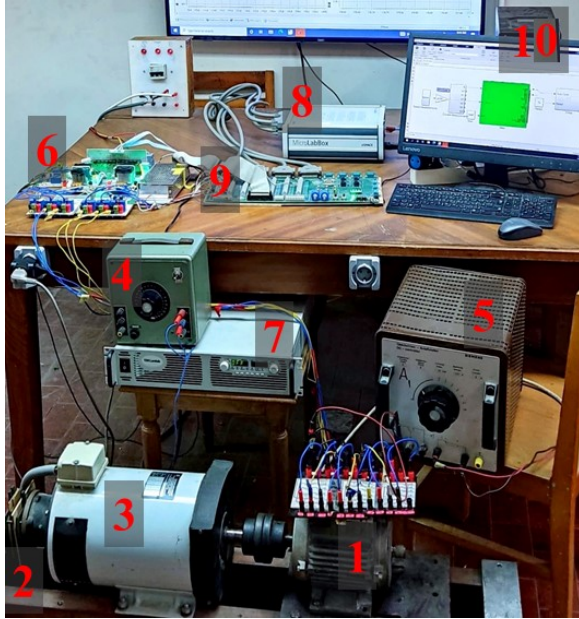
Fig. 5.   Experimental setup. 1) Six-phase motor. 2) Encoder. 3) DC generator. 4) Generator dc excitation. 5) Loading resistor. 6) Six-phase inverter. 7) DC-link programmable supply. 8) dSPACE 1202 MicroLabBox. 9) dSPACE interface board. 10) Host PC (ControlDesk).

By applying the algorithm elaborated in Section III, the mathematical representation of the $\alpha\beta$ subspace of the six-phase IM can be obtained as given by (19) to (20).

$$\frac{d}{dt}\begin{bmatrix} i_\alpha^s \\ i_\beta^s \end{bmatrix} = -\begin{bmatrix} 278.7 & 0 \\ 0 & 282.2 \end{bmatrix}\begin{bmatrix} i_\alpha^s \\ i_\beta^s \end{bmatrix} + \begin{bmatrix} 34.3 & 0 \\ 0 & 35.9 \end{bmatrix}\begin{bmatrix} v_\alpha^s \\ v_\beta^s \end{bmatrix} +$$
$$\begin{bmatrix} 501.3 & 0 \\ 0 & 500.41 \end{bmatrix}\begin{bmatrix} \lambda_\alpha^s \\ \lambda_\beta^s \end{bmatrix} + \begin{bmatrix} 0 & -1 \\ 1 & 0 \end{bmatrix}\begin{bmatrix} \omega_e i_\alpha^s \\ \omega_e i_\beta^s \end{bmatrix} + \quad (19)$$
$$\begin{bmatrix} 0 & 35.9 \\ -35.2 & 0 \end{bmatrix}\begin{bmatrix} \omega_e \lambda_\alpha^s \\ \omega_e \lambda_\beta^s \end{bmatrix}$$

$$\frac{d\omega_e}{dt} = -0.16\,\omega_e - \begin{bmatrix} 898.2 & 898.1 \end{bmatrix}\begin{bmatrix} \lambda_\alpha^s i_\beta^s \\ \lambda_\beta^s i_\alpha^s \end{bmatrix} \quad (20)$$

Based on the obtained mathematical model, the machine parameters can easily be estimated by comparing the coefficients of (19) and (20) with the canonical form given by (13) and (14). Table IV gives the estimated equivalent six-phase machine parameters assuming that the leakage inductances of both stator and rotor circuits are approximately equal. The machine is simulated using the obtained parameters and the results are compared to the experimental ones. Under this balanced case, the non-fundamental sequence current components and the corresponding torque components are ideally zero. Fig. 6 shows the fundamental $\alpha\beta$ subspace currents as well as the machine speed and developed torque. A notable agreement between the experimental and the derived model can be observed. This proves the validity of the proposed modeling approach.

TABLE IV
EQUIVALENT PARAMETERS OF FUNDAMENTAL SUBSPACE.

R_s (Ω)	4.18	L_m (H)	0.253
R_r (Ω)	3.79	J	0.0134
L_r (H) $\approx L_s$ (H)	0.268	b	0.0022

7

(a)

(b)

(c)

(d)
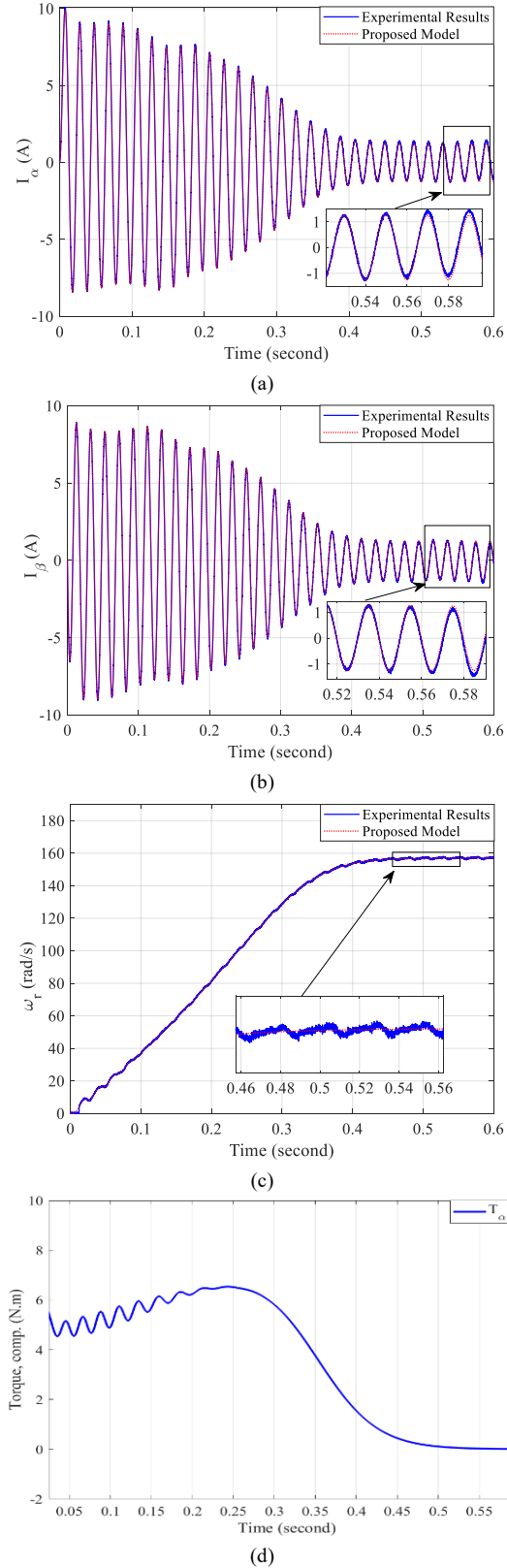
Fig. 6. Experimental and simulation results of healthy case. (a) α-subspace current. (b) β-subspace current, (c) rotor angular speed, and (d) Torque components.

TABLE V
SEQUENCE VOLTAGES UNDER UNBALANCED OPERATION

$\underline{v}^s_{\alpha\beta} = 0.68\angle0^0$	$\underline{v}^s_{xy} = 0.2\angle0^0$	$\underline{v}^s_{0^+0^-} = 0.2\angle0^0$

Case 2: Unbalanced six-phase operation

To further verify the proposed modeling approach, the mathematical model of a six-phase IM machine is obtained under unbalanced conditions and single neutral arrangement in which the xy and zero-sequence subspaces affect the dynamics. Under this case, the reference sequence voltages in per unit are given in Table V at a constant reference frequency of 50Hz, where these values are suggested to ensure that over modulation is avoided for all phases, while the magnitudes of the corresponding sequence currents are significant. This is important to obtain a good estimation accuracy for all subspaces.

The generated mathematical model under this unbalance case is given by (21) to (24). In this case, the xy sequence current components are obtained by solving (22), while those of the zero-sequence subspace are obtained using (23). Furthermore, the mechanical dynamic in (24) shows that the total developed torque has two components, namely, fundamental torque component and the torque component caused by the third harmonic flux component that is mapped to the zero subspace. Clearly, the algorithm does not result in a notable torque component from the xy subspace.

$$\frac{d}{dt}\begin{bmatrix}i^s_\alpha\\i^s_\beta\end{bmatrix} = -\begin{bmatrix}276.3 & 0\\0 & 279.3\end{bmatrix}\begin{bmatrix}i^s_\alpha\\i^s_\beta\end{bmatrix} + \begin{bmatrix}35.9 & 0\\0 & 35.8\end{bmatrix}\begin{bmatrix}v^s_\alpha\\v^s_\beta\end{bmatrix} +$$
$$\begin{bmatrix}495.2 & 0\\0 & 500.9\end{bmatrix}\begin{bmatrix}\lambda^s_\alpha\\\lambda^s_\beta\end{bmatrix} + \begin{bmatrix}0 & -1\\1 & 0\end{bmatrix}\begin{bmatrix}\omega_e i^s_\alpha\\\omega_e i^s_\beta\end{bmatrix} + \quad (21)$$
$$\begin{bmatrix}0 & 35.9\\-35.6 & 0\end{bmatrix}\begin{bmatrix}\omega_e i^s_\alpha\\\omega_e i^s_\beta\end{bmatrix}$$

$$\frac{d}{dt}\begin{bmatrix}i^s_x\\i^s_y\end{bmatrix} = -\begin{bmatrix}550 & 0\\0 & 549\end{bmatrix}\begin{bmatrix}i^s_x\\i^s_y\end{bmatrix} + \begin{bmatrix}131.5 & 0\\0 & 131.5\end{bmatrix}\begin{bmatrix}v^s_x\\v^s_y\end{bmatrix} \quad (22)$$

$$\frac{d}{dt}\begin{bmatrix}i^s_{0+}\\i^s_{0-}\end{bmatrix} = -\begin{bmatrix}197.1 & 0\\0 & 196.8\end{bmatrix}\begin{bmatrix}i^s_\alpha\\i^s_\beta\end{bmatrix} +$$
$$\begin{bmatrix}32.7 & 0\\0 & 32.6\end{bmatrix}\begin{bmatrix}v^s_{0+}\\v^s_{0-}\end{bmatrix} + \begin{bmatrix}1.4000 & 0\\0 & 1.4000\end{bmatrix}\begin{bmatrix}\lambda^s_{0+}\\\lambda^s_{0-}\end{bmatrix} + \quad (23)$$
$$\begin{bmatrix}0 & -3\\3 & 0\end{bmatrix}\begin{bmatrix}\omega_e i^s_{0+}\\\omega_e i^s_{0-}\end{bmatrix} + \begin{bmatrix}0 & 98.1\\-98.1 & 0\end{bmatrix}\begin{bmatrix}\omega_e i^s_{0+}\\\omega_e i^s_{0-}\end{bmatrix}$$

$$\frac{d\omega_e}{dt} = -0.16\,\omega_e$$
$$-\begin{bmatrix}898.5 & 897.7\end{bmatrix}\begin{bmatrix}\lambda^s_\alpha i^s_\beta\\\lambda^s_\beta i^s_\alpha\end{bmatrix} - \begin{bmatrix}2690 & 2690\end{bmatrix}\begin{bmatrix}\lambda^s_{0+} i^s_{0-}\\\lambda^s_{0-} i^s_{0+}\end{bmatrix} \quad (24)$$

Table VI shows the equivalent unbalanced six-phase machine parameters. The experimental and simulation results are compared in Figs. 7 and 8. Fig. 7(a) firstly shows the simulated average torque components under acceleration from zero, where a notable torque dip is presented around a speed of 500 rpm (one-third rated synchronous speed), which represents the effect of the 3rd harmonic component induced in the zero subspace. This is highlighted by the orange shaded ellipse in the same figure. Moreover, the corresponding speed profiles are given in Fig. 7(b), which confirms a complete consistency between the experimental data and simulations based on the developed models.

8
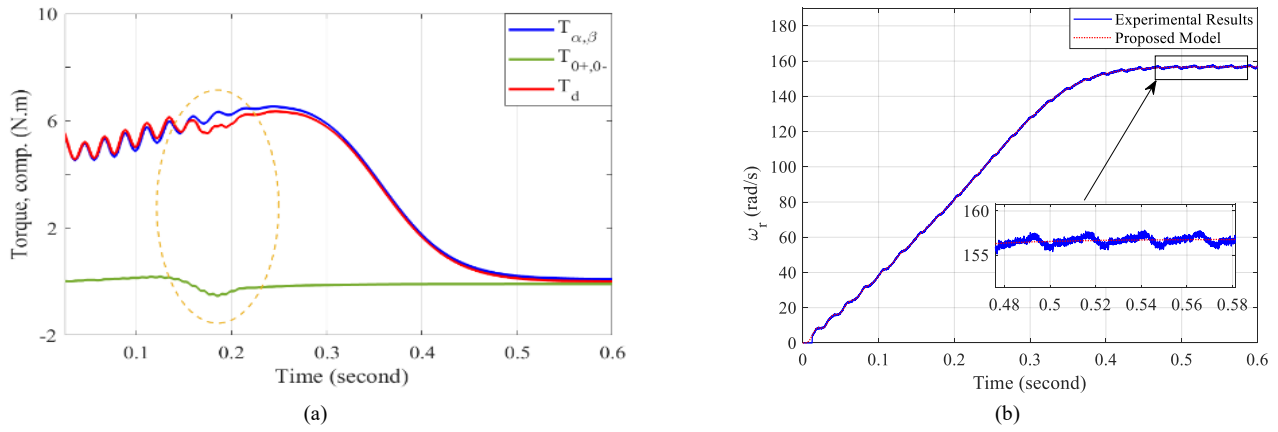
Fig. 7. Dynamic characteristics of the unbalanced six-phase machine. (a) Torque components and (b) Rotor angular speed.
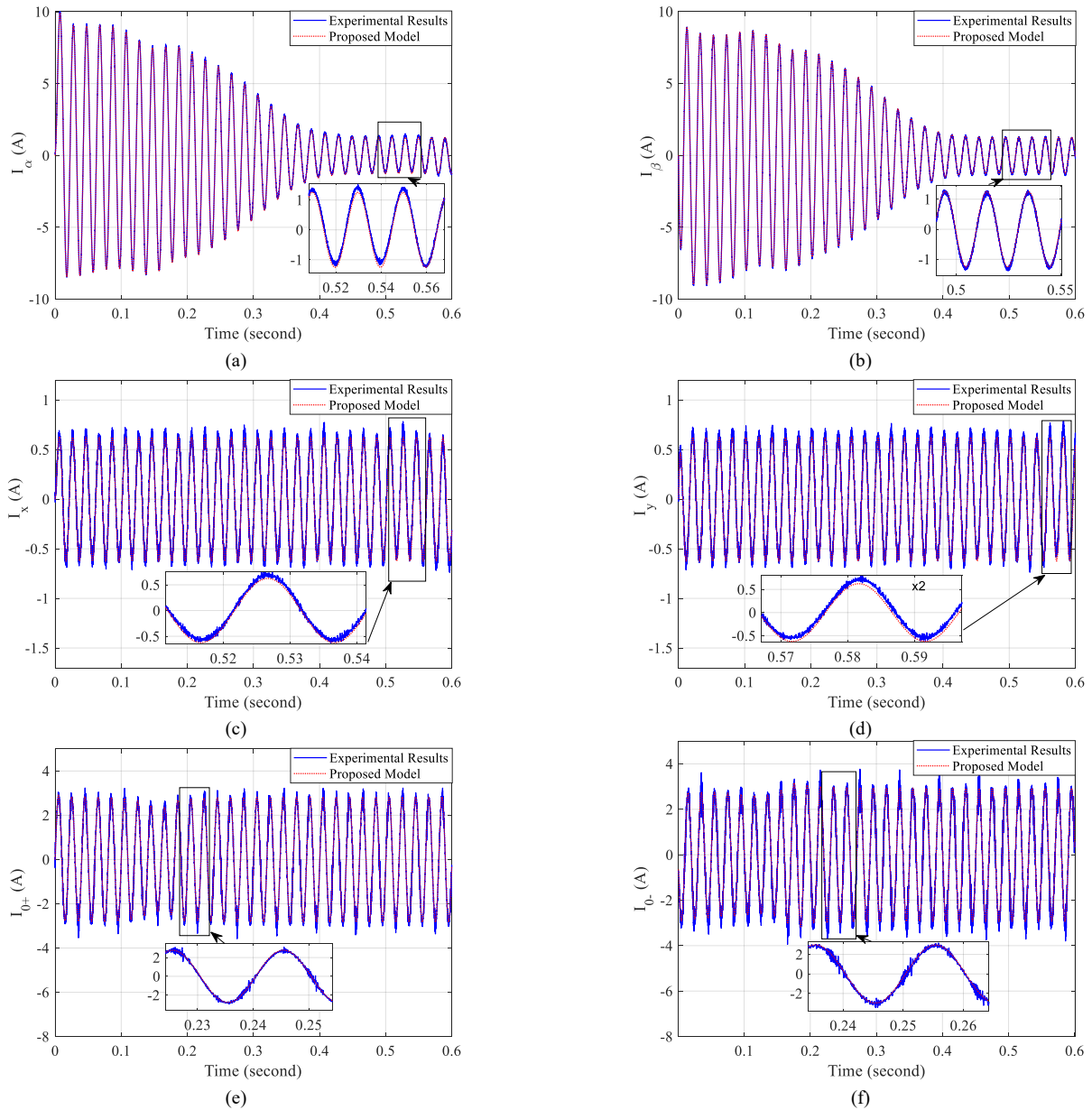
Fig. 8. Comparison between simulation and experimental results of the sequence current components under unbalanced startup. (a and b) $\alpha\beta$ current components. (c and d) xy current components. (e and f) 0_+0_- current components.

TABLE VI
UNBALANCED SIX-PHASE MACHINE PARAMETERS

Parameter	Value	Parameter	Value
R_s (Ω)	4.18	R_{r3}/L_{r3}	43.56
R_{r1} (Ω)	3.57	L_{s3} (H)	0.042
$1/\sigma_1 L_{s1}$	35.82	$L_{r3} \approx L_{s3}$ (H)	0.042
R_{r1}/L_{r1}	13.90	L_{m3} (H)	0.022
L_{s1} (H)	0.257	$L_{lr3} \approx L_{ls3}$ (H)	0.02
$L_{r1} \approx L_{s1}$ (H)	0.257	$R_{r3}(ohm)$	1.84
L_{m1} (H)	0.243	L_{s5} (H)	0.0076
$L_{ls1} = L_{lr1}$ (H)	0.014	$R_{s5}(ohm)$	4.18
$1/\sigma_3 L_{s3}$	32.71		

Fig. 8 shows the comparison between the simulated and experimental sequence current components for the three subspaces. On the one hand, the $\alpha\beta$ subspace currents are high at the starting point and show a decaying response while the machine is accelerating. On the other hand, the *xy* subspace currents almost have a constant magnitude over the whole starting period, which supports the well-established assumption in the available literature to model this subspace as a simple RL circuit. Finally, the speed voltage term caused by the third order harmonic component of the zero subspace yields this notable change in the current magnitude of the zero sequence components around one-third the rated synchronous speed.

The perfect matching between the experimental observations and the estimated model is due to setting the halting conditions for the recursive least squares regression to yield the minimum feasible error. In addition, the suggested technique incorporates several degrees of freedom and state combinations (up to second-degree polynomials) in order to attain the lowest error possible. Moreover, one of the salient features of the IM model is that the coefficients of different terms of the dynamic equations in both orthogonal directions should ideally be equal in both stationary and rotating frames due to the presumed symmetry in the machine air gap. Hence, the deviations between these coefficients during the training phase provide a general clue on the estimation inaccuracy. In the case of significant inaccuracy, the absolute and relative tolerances of the Runge-Kutta method are further increased to enhance the estimation accuracy of the flux and the governing dynamic equation at the cost of extra computational burden.

B. Computational Burden

The computational effort is an important figure of merit to assess any data-driven-based model. In the proposed model, execution time includes the time to read the data, filter it, remove DC-bias without phase distortion, estimate stator flux using the fourth order Runge-Kutta method, and estimate the model using SIDNy. It is found that the execution time is dominated by flux estimation using the fourth order Runge-Kutta method. Therefore, the execution time is recorded for different relative error tolerance for the Runge-Kutta method and is expressed in seconds, as shown in Fig. 9. Clearly, as the relative error tolerance decreases, the execution time increases. The relative tolerances of 1e-6 and 1e-7 are either recommended since they provide an accurate estimate in the shortest time possible, whereas lower values greatly increase computational time with no noticeable improvement in accuracy.
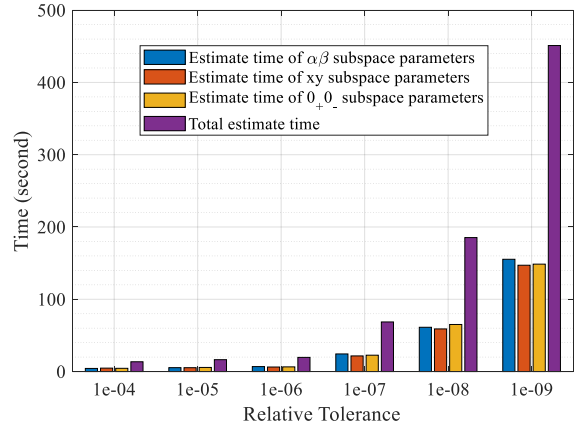
Fig. 9: Computational time for data-driven-based model of a multiphase induction machine.

C. Model Validation Under Different Operating Conditions

In this case, the estimated model has been tested using three different operating conditions, namely;
- Period I: Balanced startup condition (from 0s to 5.48s, the input voltage is 0.4 p.u. with frequency of 20 Hz at no load)
- Period II: Step speed condition (from 5.48s to 11.56s, the input voltage is 1 p.u. with frequency of 50 Hz at no load)
- Period III: Step loading condition (from 11.56s to 17s and the machine is fully loaded)

During period I, the sparse regression is utilized to estimate the machine model. Fig. 10 demonstrates that the experimental data and estimated response match adequately. In order to estimate the response during Periods II and III, the model developed in Period I is applied to the input conditions of Periods II and III. Fig. 10 shows also the dynamic characteristics of the balanced six-phase machine over the whole period. Fig. 10(a) shows the rotor speed where experimental results closely match the estimated response. Moreover, Fig. 10(b) shows the α current component of the stator current and the simulation results perfectly match the experimental results. The small mismatch during the transient periods is due to parameters detuning due to frequency change, as will be shown in following subsections.

D. Effect of Core Saturation

As a matter of fact, core saturation dramatically affects the parameters of the fundamental $\alpha\beta$ subspace, which is responsible for the fundamental flux/torque production. This effect, however, is much similar to three-phase machines and same conclusions will expectedly be obtained. In order to investigate this effect, the sparse regression is utilized to estimate the machine model for different v/f ratios, namely, 0.8 pu, 1 pu, and 1.2 pu, and Table VII displays the estimated parameters. Clearly, as the v/f ratio increases, the core is saturated and, hence, the rotor resistance, stator and mutual inductions are decreased. Since the proposed data-driven model can be updated regularly using online measurements, the effect of parameters detuning can easily be compensated for.
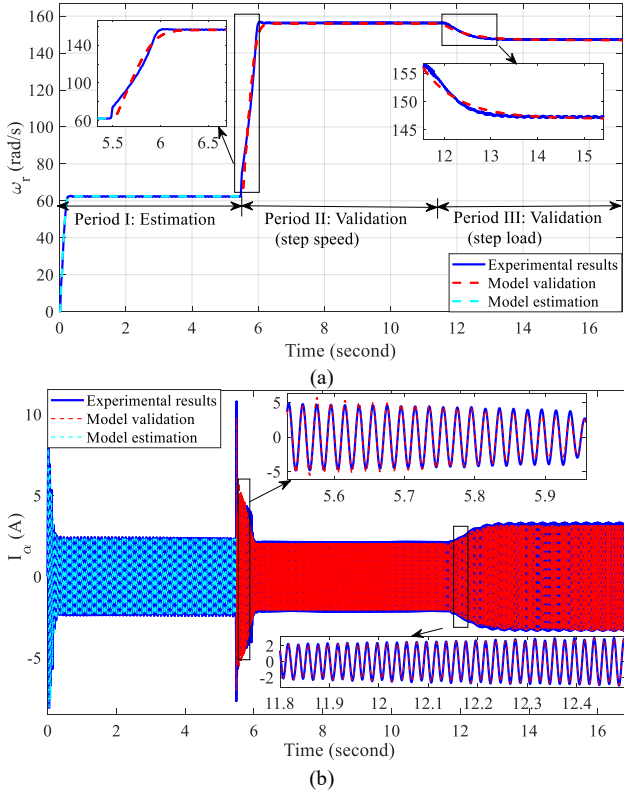
Fig. 10: Rotor angular speed of the six-phase machine during two different operating conditions.

TABLE VII
Parameters estimation under different v/f ratios.

	$v/f = 0.8\ pu$	$v/f = 1\ pu$	$v/f = 1.2\ pu$
R_s (Ω)	4.18	4.18	4.18
R_{r1} (Ω)	3.97	3.51	3.30
$1/\sigma_1 L_{s1}$	33.64	36.60	45.16
R_{r1}/L_{r1}	14.77	15.53	21.36
L_{s1} (H)	0.27	0.23	0.15
$L_{r1} \approx L_{s1}$ (H)	0.27	0.23	0.15
L_{m1} (H)	0.25	0.21	0.1
$L_{ls1} = L_{lr1}$ (H)	0.015	0.014	0.012

E. Effect of Operating Frequency

In this subsection, different operating conditions are investigated in order to estimate the machine parameters, namely, calculating the parameters while the machine is cooled at 50 Hz (starting from the ambient temperature with no prior operation warms the machine) and hot (the machine is heated from a prior operation, then it is stopped and restarted) at 50 Hz, as well as evaluating the parameters while operating at lower frequencies of 40 Hz and 30 Hz. The results are displayed in Table VIII. The table also depicts the Pearson correlation coefficient (r), which is a measure of linear correlation between sets of data and is calculated using,

$$r = \frac{\sum(x_i - \bar{x})(y_i - \bar{y})}{\sqrt{\sum(x_i - \bar{x})^2 \sum(y_i - \bar{y})^2}} \qquad (25)$$

where x_i, y_i are the values of the x-variable and y-variable in a sample, respectively. $\bar{x}, \bar{y}$ are the mean values of the x-variable and y-variable, respectively. The r value measures the strength of the relationship between the machine parameters and the frequency change. Table IX reveals that the $\alpha\beta$ subspace

parameters are highly affected with frequency. In conclusion, as the frequency drops, the values of R_{r1}, L_{s1}, and L_{m1} decrease as well. The values of R_{r1}, L_{s1}, and L_{m1} decrease by 15%, 17%, and 18%, respectively, when the frequency is decreased from 50 Hz to 40 Hz, while they are reduced by 23.8%, 20.4%, and 25.5% when the frequency is decreased from 50 Hz to 30 Hz. As clarified before, online measurements can regularly be used to improve the machine model and get better accuracy.

TABLE VIII
Parameters estimation under different operating conditions.

Frequency	50 (cooled)	50 (hot)	40	30	r
R_s (Ω)	4.18	4.18	4.18	4.18	----
R_{r1} (Ω)	3.58	4.07	3.46	3.24	0.9635
$1/\sigma_1 L_{s1}$	35.8	35.71	35.09	34.90	---
R_{r1}/L_{r1}	13.91	16.40	16.77	17.14	---
L_{s1} (H)	0.257	0.248	0.206	0.189	0.9715
$L_{r1} \approx L_{s1}$ (H)	0.257	0.248	0.206	0.189	0.9715
L_{m1} (H)	0.243	0.234	0.192	0.174	0.9713
$L_{ls1} = L_{lr1}$ (H)	0.0144	0.0144	0.0148	0.0149	-0.9449
$1/\sigma_3 L_{s3}$	32.71	30.16	34.35	33.47	---
R_{r3}/L_{r3}	43.57	39.68	47.48	47.90	---
L_{s3} (H)	0.042	0.047	0.046	0.042	0.9256
$L_{r3} \approx L_{s3}$ (H)	0.042	0.049	0.041	0.040	0.9256
L_{m3} (H)	0.022	0.0274	0.022	0.020	0.9503
$L_{ls3} = L_{lr3}$ (H)	0.020	0.021	0.019	0.02	0.5877
R_{r3} (Ω)	1.84	1.93	1.93	1.91	0.8927
L_{s5}(H)	0.0076	0.0075	0.0064	0.0061	0.9497
R_{s5} (Ω)	4.18	4.25	4.24	4.22	0.9558

F. Comparison with Harmonic-free Models.

As clarified in the introduction section, the proposed data-driven model is able to accurately model the effect of space harmonics mapped to the secondary as well as zero subspaces, which causes notable effects during transient conditions. In this subsection, the proposed model is compared with the harmonic free model, which is commonly employed in most available literature. In this latter model, the xy as well as zero subspaces are modelled using simple RL circuit. Fig. 11(a) shows the average torque components under acceleration from zero. The torque is estimated from the experimental currents based on (15). Clearly, there is notable torque dip occurring around 500 rpm (one-third of the rated synchronous speed), which represents the effect of the third harmonic component induced in the zero subspace. However, the basic RL representation on this subspace fails to represent this torque component. In addition, the corresponding current for the positive zero sequence components is shown in Fig. 11(b), which confirms a complete consistency between the experimental data and simulations based on the proposed model. However, the conventional model deviates from the actual response during the period between 0.1 and 0.2 seconds where the torque dip occurs.

V. CONCLUSION

This paper proposes a powerful sparsity-promoting technique to identify the nonlinear dynamics of multiphase induction machines (IMs) from observed states. The effectiveness of the proposed technique is demonstrated against measured noise, sensors bias, and unavailability of data

11

derivatives. Using only one transient run of the machine, this technique can effectively determine the full dynamical model of the multiphase machine. Another advantage of the proposed technique is that it can precisely retrieve machine parameters of all subspaces from the obtained model. This latter advantage represents a silent novelty over available literature, where the parameters of secondary subspaces were commonly estimated either using analytical or finite element-based analysis. Although estimated parameters generally change during operation due to several factors, the suggested technique gives an accurate dynamic model for the IM under specified conditions in which the signals are captured. Hence, online measurements can regularly be used to improve the model accuracy, which opens the door for applying the digital twin concept in electrical drive systems. Experimental validation shows a complete matching between the experimental results with the simulated machine model.

In future study, more effort will be put to provide a more computationally efficient approach to provide an adaptive online modelling using the same approach.

(a)

(b)
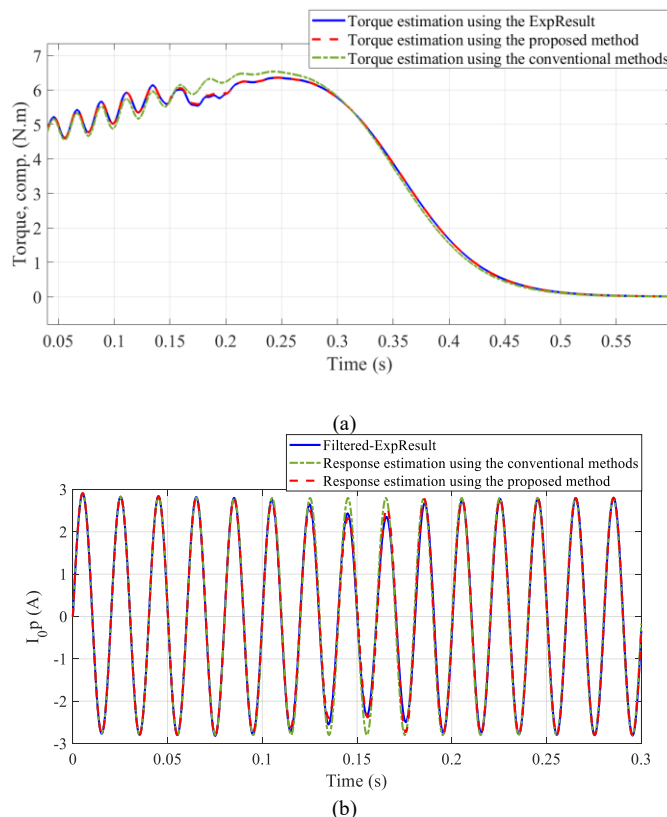
Fig. 11. Dynamic characteristics of the unbalanced six-phase machine. (a) Torque components and (b) the positive components of the zero-subspace current.

REFERENCES

[1] Y. Wang, J. Yang, R. Deng, and G. Yang, "Parameters estimation for multiphase induction machine with concentrated windings through finite element method," *IET Electric Power Applications,* vol. 14, no. 10, pp. 1807-1817, 2020.
[2] M. Perin, L. A. Pereira, L. F. A. Pereira, and G. Nicol, "Estimation of Parameters of Five-Phase Induction Motors Using Step Voltage At Standstill," *IEEE Transactions on Energy Conversion,* vol. 36, no. 4, pp. 3491-3501, 2021.
[3] J. A. Riveros *et al.*, "Parameter identification of multiphase induction machines with distributed windings—Part 2: Time-domain techniques," *IEEE Transactions on Energy Conversion,* vol. 27, no. 4, pp. 1067-1077, 2012.
[4] J. J. Guedes, M. F. Castoldi, A. Goedtel, C. M. Agulhari, and D. S. Sanches, "Parameters estimation of three-phase induction motors using differential evolution," *Electric Power Systems Research,* vol. 154, pp. 204-212, 2018.
[5] R. Babau, I. Boldea, T. Miller, and N. Muntean, "Complete parameter identification of large induction machines from no-load acceleration–deceleration tests," *IEEE transactions on industrial electronics,* vol. 54, no. 4, pp. 1962-1972, 2007.
[6] A. P. Yadav, R. Madani, N. Amiri, J. Jatskevich, and A. Davoudi, "Induction Machine Parameterization from Limited Transient Data using Convex Optimization," *IEEE Transactions on Industrial Electronics,* vol. 69, no. 2, pp. 1254-1265, 2021.
[7] J. Sun, C. Li, Z. Zheng, K. Wang, and Y. Li, "A Generalized, Fast and Robust Open-Circuit Fault Diagnosis Technique for Star-connected Symmetrical Multiphase Drives," *IEEE Transactions on Energy Conversion,* 2022.
[8] A. Habib, A. Shawier, M. Mamdouh, A. S. Abdel-Khalik, M. S. Hamad, and S. Ahmed, "Predictive current control based pseudo six-phase induction motor drive," *Alexandria Engineering Journal,* vol. 61, no. 5, pp. 3937-3948, 2022.
[9] A. S. Abdel-Khalik, A. Massoud, and S. Ahmed, "Standard three-phase stator frames for multiphase machines of prime-phase order: Optimal selection of Slot/Pole combination," *IEEE Access,* vol. 7, pp. 78239-78259, 2019.
[10] J. Paredes, B. Prieto, M. Satrústegui, I. Elósegui, and P. González, "Improving the performance of a 1-MW induction machine by optimally shifting from a three-phase to a six-phase machine design by rearranging the coil connections," *IEEE Transactions on Industrial Electronics,* vol. 68, no. 2, pp. 1035-1045, 2020.
[11] E. Levi, R. Bojoi, F. Profumo, H. A. Toliyat, and S. Williamson, "Multiphase induction motor drives – a technology status review," *IET Electric Power Applications,* vol. 1, no. 4, 2007, doi: 10.1049/iet-epa:20060342.
[12] A. S. Abdel-Khalik, M. S. Abdel-Majeed, and S. Ahmed, "Effect of winding configuration on six-phase induction machine parameters and performance," *IEEE Access,* vol. 8, pp. 223009-223020, 2020.
[13] A. S. Abdel-Khalik, A. M. Massoud, and S. Ahmed, "Nine-phase six-terminal induction machine modeling using vector space decomposition," *IEEE Transactions on Industrial Electronics,* vol. 66, no. 2, pp. 988-1000, 2018.
[14] T. Lipo, "A dq model for six phase induction machines," in *Conf. Rec. ICEM'80*, 1980.
[15] A. S. Abdel-Khalik, R. A. Hamdy, A. M. Massoud, and S. Ahmed, "Low-order space harmonic modeling of asymmetrical six-phase induction machines," *IEEE Access,* vol. 7, pp. 6866-6876, 2019.
[16] Y. Hu, Z. Zhu, and M. Odavic, "Comparison of two-individual current control and vector space decomposition control for dual three-phase PMSM," *IEEE Transactions on Industry Applications,* vol. 53, no. 5, pp. 4483-4492, 2017.
[17] M. Mengoni, S. Agarlita, L. Zarri, and D. Casadei, "On-line estimation of stator resistance and mutual inductance of multiphase induction machines," in *2012 13th International Conference on Optimization of Electrical and Electronic Equipment (OPTIM)*, 2012: IEEE, pp. 417-423.
[18] V. Kindl, R. Cermak, Z. Ferkova, and B. Skala, "Review of time and space harmonics in multi-phase induction machine," *Energies,* vol. 13, no. 2, p. 496, 2020.
[19] A. S. Abdel-Khalik, S. Ahmed, and A. M. Massoud, "Dynamic modeling of a five-phase induction machine with a combined star/pentagon stator winding connection," *IEEE Transactions on Energy Conversion,* vol. 31, no. 4, pp. 1645-1656, 2016.

[20] H. S. Che, A. S. Abdel-Khalik, O. Dordevic, and E. Levi, "Parameter estimation of asymmetrical six-phase induction machines using modified standard tests," *IEEE Transactions on Industrial Electronics,* vol. 64, no. 8, pp. 6075-6085, 2017.

[21] L. Schreier, J. Bendl, and M. Chomat, "Influence of space harmonics on properties of six-phase induction machine-Part I. analysis," in *The XIX International Conference on Electrical Machines-ICEM 2010*, 2010: IEEE, pp. 1-6.

[22] A. S. Abdel-Khalik, M. I. Daoud, S. Ahmed, A. A. Elserougi, and A. M. Massoud, "Parameter identification of five-phase induction machines with single layer windings," *IEEE Transactions on Industrial Electronics,* vol. 61, no. 10, pp. 5139-5154, 2014.

[23] M. Hannan, J. A. Ali, A. Mohamed, and A. Hussain, "Optimization techniques to enhance the performance of induction motor drives: A review," *Renewable Sustainable Energy Reviews,* vol. 81, pp. 1611-1626, 2018.

[24] F. Duan, R. Živanović, S. Al-Sarawi, and D. Mba, "Induction motor parameter estimation using sparse grid optimization algorithm," *IEEE Transactions on Industrial Informatics,* vol. 12, no. 4, pp. 1453-1461, 2016.

[25] V. Sakthivel, R. Bhuvaneswari, and S. Subramanian, "Multi-objective parameter estimation of induction motor using particle swarm optimization," *Engineering Applications of Artificial Intelligence,* vol. 23, no. 3, pp. 302-312, 2010.

[26] J. Abd Ali, M. Hannan, A. Mohamed, and M. G. Abdolrasol, "Fuzzy logic speed controller optimization approach for induction motor drive using backtracking search algorithm," *Measurement,* vol. 78, pp. 49-62, 2016.

[27] R.-C. Wu, Y.-W. Tseng, and C.-Y. Chen, "Estimating parameters of the induction machine by the polynomial regression," *Applied Sciences,* vol. 8, no. 7, p. 1073, 2018.

[28] D. Gutierrez-Reina, F. Barrero, J. Riveros, I. Gonzalez-Prieto, S. L. Toral, and M. J. Duran, "Interest and applicability of meta-heuristic algorithms in the electrical parameter identification of multiphase machines," *Energies,* vol. 12, no. 2, p. 314, 2019.

[29] B. Mahesh, "Machine learning algorithms-a review," *International Journal of Science Research* vol. 9, pp. 381-386, 2020.

[30] M. Z. Ali, M. N. S. K. Shabbir, S. M. K. Zaman, and X. Liang, "Single- and multi-fault diagnosis using machine learning for variable frequency drive-fed induction motors," *IEEE Transactions on Industry Applications,* vol. 56, no. 3, pp. 2324-2337, 2020.

[31] I. Martin-Diaz, D. Morinigo-Sotelo, O. Duque-Perez, and R. J. Romero-Troncoso, "An experimental comparative evaluation of machine learning techniques for motor fault diagnosis under various operating conditions," *IEEE Transactions on Industry Applications,* vol. 54, no. 3, pp. 2215-2224, 2018.

[32] A. G. Yepes *et al.*, "Parameter identification of multiphase induction machines with distributed windings—Part 1: Sinusoidal excitation methods," *IEEE Transactions on Energy Conversion,* vol. 27, no. 4, pp. 1056-1066, 2012.

[33] S. L. Brunton, J. L. Proctor, and J. N. Kutz, "Discovering governing equations from data by sparse identification of nonlinear dynamical systems," *Proceedings of the national academy of sciences,* vol. 113, no. 15, pp. 3932-3937, 2016.

[34] F. Baneira, J. Doval-Gandoy, A. G. Yepes, O. Lopez, and D. Pérez-Estévez, "Control strategy for multiphase drives with minimum losses in the full torque operation range under single open-phase fault," *IEEE Transactions on Power Electronics,* vol. 32, no. 8, pp. 6275-6285, 2016.

Mohamed A. Abu-seif received the B.Sc. degree in electrical engineering from Alexandria University, Alexandria, Egypt, in 2021. He is currently a master's student at Alexandria University, Alexandria, Egypt. And a systems engineer at Brightskies. His current research interest includes electrical automotive powertrain systems, lithium-ion battery management systems, electric drives, dynamical system modeling.

MOHAMED AHMED received the B.Sc. degree in Electrical Engineering from Alexandria University, Alexandria, Egypt, in 2016. He is currently a Teaching Assistant with the Mathematics and Applied Physics Department, Faculty of Engineering, Alexandria University, Alexandria, Egypt. His current research interests include renewable energy, smart grids, power system control.

Mohamed Y. Metwly (M'21) received the B.Sc. degree in electrical engineering from Alexandria University, Alexandria, Egypt, in 2018, and the M.Sc. in smart grid engineering from the Arab Academy for Science, Technology and Maritime Transport (AAST), Alexandria, Egypt, in 2022. He is currently a Ph.D. student and research assistant in electrical engineering at the AMPERE Lab, University of Kentucky (UK), USA. His current research interests include machine design, battery chargers, electric vehicles, renewable energy systems, and multi-objective optimization.

Ayman S. Abdel-Khalik (SM'12) received the B.Sc. and M.Sc. degrees in electrical engineering from Alexandria University, Alexandria, Egypt, in 2001 and 2004, respectively, and the Ph.D. degree in electrical engineering from Alexandria University, and Strathclyde University, Glasgow, U.K., in 2009, under a dual channel program. He is currently a Professor with the Electrical Engineering Department, Faculty of Engineering, Alexandria University, Alexandria, Egypt. He serves as an Associate Editor of IEEE Transactions on Industrial Electronics. Also, he serves as the Editor-in-Chief of Alexandria Engineering Journal. His current research interests include electrical machine design and modelling, electric drives, energy conversion, and renewable energy.

Mostafa Hamad (SM'19) obtained the B.Sc. and M.Sc. degrees in Electrical Engineering from Alexandria University, Alexandria, Egypt, in 1999 and 2003, respectively, and the Ph.D. degree in Electrical Engineering from Strathclyde University, Glasgow, U.K., in 2009. Currently he is a Professor in the Department of Electrical and Control Engineering, College of Engineering and Technology, Arab Academy for Science, Technology and Maritime Transport (AASTMT), Alexandria, Egypt. His research interests include power electronics applications in power quality, electric drives, distributed generation, HVDC transmission, and renewable energy.

Shehab Ahmed (SM'12) received the B.Sc. degree in electrical engineering from Alexandria University, Alexandria, Egypt, in 1999, and the M.Sc. and Ph.D. degrees from the Department of Electrical and Computer Engineering, Texas A&M University, College Station, TX, USA, in 2000 and 2007, respectively. He was with Schlumberger Technology Corporation, Houston, TX, USA, from 2001 to 2007, developing downhole mechatronic systems for oilfield service products. He was with Texas A&M University at Qatar from 2007 to 2018. He is currently Professor and Program Chiar of the Electrical and Computer Engineering program in the CEMSE Division at King Abdullah University of Science and Technology (KAUST), Saudi Arabia. His research interests include mechatronics, solid-state power conversion, and electric machines.

Noha Elmalhy received the B.Sc. and M.Sc. degrees in electrical engineering from Alexandria University, Alexandria, Egypt, in 2005 and 2010, respectively, and the Ph.D. degree in electrical engineering from Alexandria University in 2017. She is currently a Lecturer with the Electrical Engineering Department, Faculty of Engineering, Alexandria University, Alexandria, Egypt. Her current research interests include electrical machine and drives, energy conversion, and renewable energy.